that a 1,2 shift mechanism operates in $C_8H_8Fe(CO)_3$.
(4) G. Rigatti, G. Baccalon, A. Ceccon, and G. Giacometti, *J. Chem. Soc., Chem. Commun.*, 1165 (1972).
(5) C. G. Kreiter, A. Maasbol, F. A. L. Anet, H. D. Kaesz, and S. Winstein, *J. Am. Chem. Soc.*, **88**, 3444 (1966).
(6) (a) F. A. L. Anet, H. D. Kaesz, A. Maasbol, and S. Winstein, *J. Am. Chem. Soc.*, **89**, 2489 (1967); (b) F. A. L. Anet, *ibid.*, **89**, 2491 (1967).
(7) R. Grubbs, R. Breslow, R. Herber, and S. J. Lippard, *J. Am. Chem. Soc.*, **89**, 6864 (1967).
(8) B. Dickens and W. N. Lipscomb, *J. Chem. Phys.*, **37**, 2084 (1962).
(9) W. K. Bratton, F. A. Cotton, A. Davison, A. Musco, and J. W. Faller, *Proc. Natl. Acad. Sci. U.S.A.*, **58**, 1324 (1967).
(10) F. A. Cotton, A. Davison, T. J. Marks, and A. Musco, *J. Am. Chem. Soc.*, **91**, 6598 (1969).
(11) J. B. Stothers, "Carbon-13 NMR Spectroscopy", Academic Press, New York, N.Y., 1972, p 421.
(12) T. A. Manuel and F. G. A. Stone, *J. Am. Chem. Soc.*, **82**, 366 (1960).
(13) M. D. Rausch and G. N. Schrauzer, *Chem. Ind. (London)*, 957 (1959).
(14) B. F. G. Johnson, J. Lewis, and M. U. Twigg, *J. Organomet. Chem.*, **67**, C75 (1974).
(15) L. Kruczynski, J. L. Martin, and J. Takats, *J. Organomet. Chem.*, **80**, C9 (1974).
(16) F. Calderazzo and F. L'Eplattenier, *Inorg. Chem.*, **6**, 1220 (1967).
(17) F. A. Cotton and R. Eiss, *J. Am. Chem. Soc.*, **91**, 6593 (1969).
(18) F. A. Cotton, D. L. Hunter, and P. Lahuerta, *J. Am. Chem. Soc.*, **96**, 7926 (1974).
(19) G. C. Levy and G. L. Nelson, "Carbon-13 Nuclear Magnetic Resonance for Organic Chemist", Wiley, New York, N.Y., 1972, pp 59–68.
(20) H. G. Preston, Jr., and J. C. Davis, Jr., *J. Am. Chem. Soc.*, **88**, 1585 (1966).
(21) H. L. Retcofsky, E. N. Frankel, and H. S. Gutowsky, *J. Am. Chem. Soc.*, **88**, 2710 (1966).
(22) J.-Y. Lallemand, P. Lazlo, C. Muzette, and A. Stockis, *J. Organomet. Chem.*, **91**, 71 (1975).
(23) F. A. Cotton, G. Deganello, D. L. Hunter, P. L. Sandrini, and B. R. Stults, unpublished data on various $Fe(CO)_3$ and $Ru(CO)_3$ containing systems.
(24) J. Takats and L. Kruczynski, *J. Am. Chem. Soc.*, **96**, 932 (1974).
(25) C. G. Kreiter and M. Lang, *J. Organomet. Chem.*, **55**, C27 (1973).
(26) F. A. Cotton, D. L. Hunter, and P. Lahuerta, *J. Am. Chem. Soc.*, **97**, 1046 (1975).
(27) F. A. Cotton, D. L. Hunter, and P. Lahuerta, *J. Organomet. Chem.*, **87**, C42 (1975).
(28) F. A. Cotton, D. L. Hunter, and P. Lahuerta, *Inorg. Chem.*, **14**, 511 (1975).
(29) R. D. Adams, F. A. Cotton, W. R. Cullen, D. L. Hunter, and L. Mihichuk, *Inorg. Chem.*, **14**, 1395 (1975).
(30) The reasoning used to justify, or rationalize its occurrence for the (η^6-C_8H_8)$M(CO)_3$ species is such that it would be predicted to occur in (η^6-C_8H_8)ML_n species in general, and also in (η^5-C_7H_7)ML_n species. These predictions are being tested by F.A.C. and John R. Kolb.
(31) See, for example, F. A. Cotton, "Chemical Applications of Group Theory", 2d ed, Wiley, New York, N.Y., 1971, pp 147–148.
(32) F. A. Cotton, J. W. Faller, and A. Musco, *J. Am. Chem. Soc.*, **90**, 1438 (1968).
(33) The more speculative the argument the briefer it should be. Lemma: Totally speculative argument deserves no space at all.

Calculation of the Ground State Electronic Structures and Electronic Spectra of Di- and Trisulfide Radical Anions by the Scattered Wave–SCF–Xα Method

F. Albert Cotton,* Jane B. Harmon, and Richard M. Hedges*

Contribution from the Department of Chemistry, Texas A&M University, College Station, Texas 77843. *Received July 21, 1975*

Abstract: In order to get additional, and independent, evidence concerning the identity of the S_n^- species responsible for the blue color of lapis lazuli, sulfur-doped alkali halide crystals, and certain solutions of sulfur in alkalies, the SCF-scattered wave-Xα method has been used to calculate the ground state electronic structures and the electronic absorption spectra of S_2^-, S_3^-, and S_3^{2-}. The latter was used as a check on the method, and excellent agreement between the observed (~24 000 cm^{-1}) and calculated (~24 500 cm^{-1}) energies of the lowest allowed singlet-singlet electronic absorption band was obtained. For the S_2^- and S_3^- species the first allowed doublet-doublet transition is predicted to occur at 17 300–20 300 cm^{-1} (depending on structure parameters) and 12 000–13 200 cm^{-1} (again depending on structure parameters). Since the blue sulfur-containing systems have an absorption band with an origin at ca. 13 500 cm^{-1} we conclude that the blue chromophore is S_3^-. Likewise, sulfur-doped alkali halide crystals that are pink have an absorption band with an origin at ca. 21 000 cm^{-1} so that the pink color may be attributed to the presence of S_2^-.

The problem we are addressing here has a history dating from the time of Marco Polo (1271) and before. This is the question of how to account for the deep blue color of minerals known from early times as lapis lazuli, and, in the synthetic forms now available, as ultramarine. These substances have long been prized for their beautiful color, and lapis lazuli is still collected from nature today, the principal regions of occurrence being Badakhshan in northeast Afganistan and near the western end of Lake Baikal in the USSR.

In recent times it has been established that the principal component of lapis lazuli and ultramarines is a silicate mineral of the sodalite type[1] containing small amounts of sulfur. It has also been known for some time that a blue color develops when sulfur is heated with water and a trace of basic salt.[2-4] Blue solutions are also formed by sulfur in alkali halide melts,[5,6] on dissolving alkali polysulfides in basic solvents such as dimethylformamide[7,8] and dimethyl sulfoxide,[9] upon doping sulfur into borate glasses,[10] upon electrochemical reduction of S_8 in dimethyl sulfoxide,[11,12] and upon heating alkali halide crystals in sulfur vapors,[13,14] although with some crystals a pink color rather than the deep blue color is formed. In all cases which have been examined spectrophotometrically, the cause of the blue color has been shown to be an absorption band centered at about 625 nm (16 000 cm^{-1}).

Efforts to identify the species responsible for the blue color have been numerous. Lux and co-workers[7,9] attributed it to neutral molecules S_x, $x = 2, 3, 4$. Merritt and Sawyer[11] once suggested that S_8^- is the species formed by electrochemical reduction of elemental sulfur in dimethyl sulfoxide but later retracted[15] this suggestions and agreed with Bonnaterre and Cauquis[12] who showed that the oxidation number in this system is $-\frac{1}{3}$ and proposed S_6^{2-} as the chromophore. Chivers and Drummond[16,17] agreed that the blue species corresponds formally to S_6^{2-} but proposed that its real identity is S_3^-. Gruen, McBeth, and Zielen[6] also propose that the blue color is caused by S_3^-, but Giggenbach[4,8,10] has argued in favor of S_2^-. Hofmann et al.[18] in discussing ultramarine specifically suggest that either S_2^-

or S_3^-, or both, might be the blue chromophore.

A study conducted by Chivers and Drummond[16] on solutions of polysufides in hexamethylphosphoramide and very dilute solutions of elemental sulfur gave similar spectra with the same relative intensities of the peaks at 16 100 and 36 200 cm^{-1}. After electrical transference, identical spectra are obtained from the blue solutions, which was taken to indicate that the two peaks are due to one negatively charged species. It was suggested that the sulfur is being reduced rather than disproportionating to give the blue species. An analysis of the dependence of the absorption coefficient at 16 100 cm^{-1} on concentration, in terms of possible equilibria between various S_x^{2-} and S_x^- species, led Chivers and Drummond to conclude that the S_3^- ion is the blue species.

A study of a 2.5×10^{-3} M solution of sodium tetrasulfide in a 0.2 M HS^--H_2S buffer solution at pH 5.6 as a function of temperature has been reported by Giggenbach.[4] At room temperature, the absorption spectra of aqueous polysulfide solutions show two bands[19,20] in the near-uv region at 25 000 and 31 000 cm^{-1}. Up to about 100 °C, these two bands were observed to move toward lower energies without any significant change in either the shape or the molar absorptivity at the absorption maxima. At temperatures above 100 °C, however, a new band appeared around 16 500 cm^{-1} and increased in intensity with increasing temperature, causing the color of the solution to change from yellow through green to blue. The temperature dependence of the spectra for a series of sodium tetrasulfide solutions in a number of dimethylformamide (DMF) and water mixtures demonstrated that decreasing DMF content led to an increase in the temperature required to produce a certain amount of the blue species as indicated by its characteristic absorption. Therefore, the species formed in aqueous solution was assumed to be the S_2^- ion, and the equilibrium at elevated temperatures was formulated as

$$S_3S^{2-} = 2S_2^-$$

with the possibilities of the blue color being due to uncharged[21] or doubly charged[22] particles excluded. On the other hand, Giggenbach argued that the nonexistence of polysulfide ions S_nS^{2-} with $n > 5$ in aqueous solution[23] requires that the number of sulfur atoms (m) of the dissociation product S_m^- not exceed three,[11] which reduces the number of possible species[23] to S_2^- and S_3^-. Then, in view of the very small amount of S_3^- ion observed[8,12] in DMF and dimethyl sulfoxide (DMSO) solutions he suggested that S_2^- predominates in these systems. Electronic spin resonance investigations on sulfur-doped borate glasses[10,24] and on ultramarine[25] reveal the existence of significant amounts of S_3^- ions. Since no additional absorption band attributable to this ion is detected in these systems, Giggenbach suggested that the absorption spectrum of S_3^- is similar to that of S_2^-, thus implying that S_3^- is also blue.[23]

A study of Raman spectra of S_2^- and S_3^- doped in alkali halide crystals is reported by Holzer, Murphy, and Bernstein.[26] Their findings support previous identification of a diatomic species S_2^-[27,28] and a bent triatomic species S_3^-.[13,14] The observed Raman spectra of sulfur-doped KI show two bands at 543 and 594 cm^{-1}. The visible absorption spectrum of this crystal shows two bands at approximately 25 000 and 16 000 cm^{-1}. Irradiation of the crystal with ultraviolet light causes the Raman band at 543 cm^{-1} and the visible absorption at 16 000 cm^{-1} to disappear. This suggests the following association: 594 cm^{-1} with 25 000 cm^{-1} and 543 cm^{-1} with 16 000 cm^{-1}. After irradiation, the ir absorption band previously found at 585 cm^{-1} was gone, indicating that the species remaining is diatomic and symmetrical. ESR indicated that the remaining species was S_2^-, as previously identified.[28] The species which disappears on irradiation has a Raman band at 546 cm^{-1}, an ir absorption band at 585 cm^{-1}, and a visible absorption band at 16 000 cm^{-1}. The noncoincident ir and Raman frequencies indicate that this species has more than two atoms. Further evidence for associating the Raman line at 543 cm^{-1} with the visible absorption band at 16 000 cm^{-1} was obtained from the following observation in which a resonance Raman enhancement effect is involved. When the Raman exciting line was moved from 20 500 to 19 400 cm^{-1}, that is, more into the 16 000-cm^{-1} visible band, it was the 543-cm^{-1} Raman band that gained intensity while the 594-cm^{-1} Raman band lost intensity.

Holzer and co-workers[26] predict that the shift in vibrational frequencies of the $(^{32}S^{34}S)^-$ band from the $^{32}S_2^-$ band should be −1.56%. For doped NaCl, a band at 531 cm^{-1} is observed at higher resolution. A shoulder due to $(^{32}S^{34}S)^-$ is shifted 5.6 cm^{-1}, that is, only -1.0 ± 0.1%. They take this as further evidence that this band is not due to a diatomic species. These results also suggest that the band is not due to a linear triatomic species, in which case the same isotopic shift as in the diatomic case should then be observed, since the Raman band is due to the symmetric stretch in which only the two outer atoms move. Previous ESR studies[29] suggesting the presence of S_3^- in the mineral ultramarine are supported by Holzer and co-workers through their observation of a Raman band at 546 cm^{-1} and a weak shoulder at 570 cm^{-1}. The band at 546 cm^{-1} was not observed in sodalite, which has the same host structure but contains no sulfur.

From the foregoing summary it is clear that although the sulfur–polysulfide systems have been studied extensively, the identity of the blue species has not been conclusively determined. While the case in favor of the S_3^- ion appears to be rather good, we feel that the evidence is still not conclusive. A study of the electronic structures of the polysulfide radical ions was therefore undertaken using the SCF-Xα scattered-wave method with the objective of obtaining independent evidence concerning the spectral assignments. It is our opinion that this method is well suited to the treatment of the small, homonuclear species with which we are here concerned.

Procedure for Calculations

The SCF-Xα scattered-wave method[30] was used to determine the electronic structures of the polysulfide ions S_3^-, S_2^-, and S_3^{2-}. The coordinate systems used for the trisulfide ions and the disulfide ion are shown in Figure 1. The outer sphere was centered at the weighted-average position of all the atoms, where the weights were the number of valence electrons in the neutral free atoms. The α exchange parameter for sulfur was taken from the tabulation of Schwarz.[31] For the extramolecular and intersphere regions, the atomic α's were averaged with the same weights used in determining the outer sphere center. All of the calculations performed on the polysulfides include s-, p-, and d-type spherical harmonics on sulfur to expand the wave functions. Overlapping atomic and outer sphere radii were obtained by the nonempirical procedure recently suggested by Norman.[32] Throughout the calculation, the stabilizing influence of a surrounding crystal lattice on the polysulfide ions was simulated by adding to the potential that of a "Watson sphere"[33] with radius equal to that of the outer sphere. In each calculation, the final SCF ground state potential was used to search for excited state energy levels up to a maximum energy of 0.0020 Ry. This potential was then used as the starting potential for SCF calculations of the electronic transition energies using Slater's transition-state concept.[30a,34]

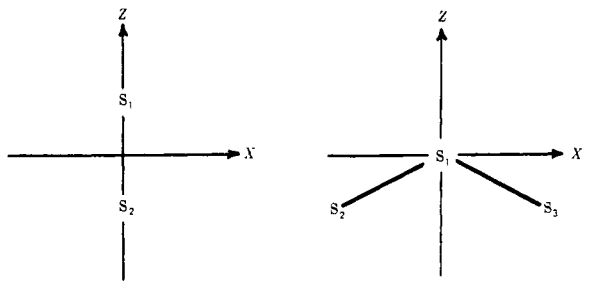

Figure 1. Coordinate systems used for (a) the S_2^- ion and, (b) the S_3^- and S_3^{2-} ions.

SCF Calculation of S_3^-. Two complete calculations (hereafter $S_3^-(1)$ and $S_3^-(2)$) were performed on S_3^-. The first, $S_3^-(1)$, assumed the bond length S–S = 2.10 Å and the second, $S_3^-(2)$, assumed S–S = 2.00 Å. In both cases the angle formed by the three sulfur atoms was set at 110°.[17,35] Coordinates, α parameters, and sphere radii are summarized in Table I. Symmetry (C_{2v}) was employed to factor the secular matrix into a_1, a_2, b_1, and b_2 blocks. In both calculations the initial molecular potential was constructed by superposition of SCF–Xα charge densities for free $S^{0.33-}$. The "Watson sphere" used in these calculations contained one unit of positive charge uniformly distributed over its surface, with its radius equal to that of the outer sphere. The ground state one-electron eigenvalues converged within 0.10% in 32 and 38 iterations for $S_3^-(1)$ and $S_3^-(2)$, respectively. An average of the former and new potentials in a 9:1 ratio, respectively, for a given iteration was used as the starting potential for the next iteration. Core levels (sulfur 1s, 2s, and 2p) were frozen through the first 19 iterations for $S_3^-(1)$ and first 18 iterations for $S_3^-(2)$, and thereafter calculated explicitly using only the potential within the sphere surrounding the atom in question. The final ground state potential was used as the starting point for SCF calculations of transition energies. These calculations were done in spin-unrestricted form to obtain predictions for the electronic excitations.

SCF Calculation of S_2^-. Two complete calculations (hereafter $S_2^-(1)$ and $S_2^-(2)$) were performed on S_2^-. The first, $S_2^-(1)$, assumed the bond length S–S = 2.10 Å and the second assumed S–S = 2.25 Å. In both cases, the outer sphere was centered at the inversion center of the molecule. Coordinates, α parameters, and sphere radii are summarized in Table I. The molecular orbitals were constructed according to the conventional methods used for homonuclear diatomics, and the secular matrix was factored into σ_g, σ_u, π_g, and π_u symmetry blocks. In both cases the initial molecular potential was constructed by superposition of SCF–Xα charge densities for free $S^{0.5-}$. The "Watson sphere" used in these calculations contained one unit of positive charge uniformly distributed over its surface, with its radius equal to that of the outer sphere. The ground state one-electron eigenvalues converged within 0.10% in 38 iterations and 33 iterations for $S_2^-(1)$ and $S_2^-(2)$, respectively. An average of the former and new potentials in a 9:1 ratio, respectively, for a given iteration was used as the starting potential for the next iteration. Core levels (sulfur 1s, 2s, and 2p) were frozen through the first five iterations for both $S_2^-(1)$ and $S_2^-(2)$, and thereafter calculated explicitly using only the potential within the sphere surrounding the atom in question. The final ground state potential was used as the starting point for SCF calculations of transition energies. These calculations were done in spin-unrestricted form to obtain predictions for the electronic excitations.

SCF Calculation of S_3^{2-}. One complete calculation was performed on S_3^{2-} employing experimental bond parameters,[36-38] namely, S–S = 2.15 Å and an SSS angle of 103°. Coordinates, α parameters, and sphere radii are summarized in Table I. Again, symmetry (C_{2v}) was employed to factor the secular matrix into a_1, a_2, b_1, and b_2 blocks. The initial molecular potential was constructed by superposition of SCF–Xα charge densities for free $S^{0.66-}$. The "Watson sphere" in these calculations contained two units of positive charge uniformly distributed over its surface, with its radius equal to the outer sphere radius. The ground state one-electron eigenvalues converged within 0.10% in 13 iterations. An average of the former and new potentials in a 9:1 ratio, respectively, for a given iteration was used as the starting potential for the next iteration. Core levels (sulfur 1s, 2s, and 2p) were frozen through the first eight iterations and thereafter calculated explicitly using only the potential within the sphere surrounding the atom in question. The final ground state potential was used as the starting point for SCF calculations of transition energies. These calculations were done first in spin-restricted form, to obtain a weighted-average energy for the singlet and triplet components of a given transition, and then in spin-unrestricted form, to obtain a separate prediction for the triplet. Combination of the two results gives an explicit prediction of the singlet transition energy.

Table I. Atomic Coordinates, α Parameters, and Sphere Radii (Atomic Units)

Species	Region	x	y	z	α	R
$S_3^-(1)$	S_1	0	0	0	0.72475	2.05832
	S_2	−3.25071	0	−2.27618	0.72475	2.23086
	S_3	3.25071	0	−2.27618	0.72475	2.23086
	Extra-molecular	0	0	−1.51750	0.72475	5.40235
$S_3^-(2)$	S_1	0	0	0	0.72475	1.87000
	S_2	−3.09595	0	−2.16781	0.72475	2.03184
	S_3	3.09595	0	−2.16781	0.72475	2.03184
	Extra-molecular	0	0	−1.44520	0.72475	5.14727
$S_2^-(1)$	S_1	0	0	1.98421	0.72475	2.04847
	S_2	0	0	−1.98421	0.72475	2.04847
	Extra-molecular	0	0	0	0.72475	3.96843
$S_2^-(2)$	S_1	0	0	2.12594	0.72475	2.19479
	S_2	0	0	−2.12594	0.72475	2.19479
	Extra-molecular	0	0	0	0.72475	4.25189
S_3^{2-}	S_1	0	0	0	0.72475	2.05832
	S_2	−3.17959	0	−2.52940	0.72475	2.23086
	S_3	3.17959	0	−2.52940	0.72475	2.23086
	Extra-molecular	0	0	−1.68628	0.72475	5.40256

Results

The S_3^- Calculations. The two calculations, $S_3^-(1)$ and $S_3^-(2)$, were performed in spin-unrestricted form because of the open-shell nature of the ion. Calculated ground state valence orbital energies and charge distributions are summarized for $S_3^-(1)$ and $S_3^-(2)$ in Table II. Calculated core one-electron energies are given in Table III. The spin-polarized SCF–Xα electronic energy levels of the $S_3^-(2)$ ion are shown in Figure 2. The levels are labeled according to the irreducible representations of the C_{2v} symmetry group. The highest occupied level in the ground state is $2b_2\uparrow$. Summarized in Table IV are the calculated all-electron energies and charge distributions. A contour map of the one-electron wave function for the highest occupied level ($2b_2\uparrow$) in $S_3^-(2)$ appears as Figure 3. It should be emphasized that this contour map has not been generated from linear combinations of analytic atomic orbitals of the type traditionally used in Hartree–Fock molecular orbital theory. It has been generated simply from the numerical values of the wave

Table II. Ground State Valence Energy Levels[a] (Rydbergs) and Charge Distribution[b] for S_3^-[c]

Level	Energy	% S_1	% $S_{2,3}$	Level	Energy	% S_1	% $S_{2,3}$
$4b_1\downarrow$	−0.140, −0.108	29.3, 24.9	34.7, 29.9	$1b_2\downarrow$	−0.634, −0.665	34.4, 29.3	23.7, 23.1
$4b_1\uparrow$	−0.160, −0.131	29.6, 25.7	35.5, 31.2	$1b_2\uparrow$	−0.654, −0.682	35.6, 32.2	22.9, 29.1
$5a_1\downarrow$	−0.194, −0.176	20.7, 12.7	37.1, 23.4	$3a_1\downarrow$	−0.661, −0.689	37.3, 32.5	29.6, 23.3
$5a_1\uparrow$	−0.212, −0.194	21.2, 14.1	38.6, 26.4	$3a_1\uparrow$	−0.682, −0.708	38.1, 33.3	29.3, 28.7
$2b_2\downarrow$	−0.404, −0.400	26.5, 25.7	40.3, 35.4	$2b_1\downarrow$	−0.706, −0.724	31.6, 27.8	43.4, 42.4
$2b_2\uparrow$	−0.424, −0.425	25.9, 25.1	41.3, 36.5	$2b_1\uparrow$	−0.727, −0.749	32.0, 28.4	43.2, 42.2
$3b_1\downarrow$	−0.465, −0.472	0.9, 1.1	67.6, 62.9	$2a_1\downarrow$	−1.124, −1.125	26.9, 26.4	54.6, 50.3
$3b_1\uparrow$	−0.482, −0.492	0.9, 1.1	67.8, 63.2	$2a_1\uparrow$	−1.145, −1.151	26.3, 25.8	55.3, 51.0
$1a_2\downarrow$	−0.493, −0.510	0.7, 0.7	64.0, 58.9	$1b_1\downarrow$	−1.268, −1.298	5.8, 6.3	76.5, 71.7
$4a_1\downarrow$	−0.497, −0.512	7.0, 8.6	57.5, 50.8	$1b_1\uparrow$	−1.287, −1.321	5.9, 6.5	76.5, 71.6
$1a_2\uparrow$	−0.511, −0.523	0.7, 0.8	64.4, 59.2	$1a_1\downarrow$	−1.464, −1.512	48.9, 44.1	31.0, 31.2
$4a_1\uparrow$	−0.515, −0.533	6.7, 8.2	58.0, 51.4	$1a_1\uparrow$	−1.488, −1.541	49.8, 45.2	30.3, 30.2

[a] The highest occupied level is $2b_2\uparrow$. [b] The remainder of the electronic charge is distributed between the intersphere and extramolecular regions (not listed here). [c] Results for $S_3^-(1)$ and $S_3^-(2)$ are given side by side in that order.

Table III. Ground State Core Energy Levels (Ry) for S_3^-

Level	Energy $S_3^-(1)$	Energy $S_3^-(2)$
S_1 1s↑	−177.3774	−177.4503
S_1 1s↓	−177.3722	−177.4432
S_1 2s↑	−15.0957	−15.1354
S_1 2s↓	−15.0895	−15.1271
S_1 2p↑	−11.3300	−11.3732
S_1 2p↓	−11.3225	−11.3630
$S_{2,3}$ 1s↑	−177.0650	−177.0079
$S_{2,3}$ 1s↓	−177.0617	−177.0040
$S_{2,3}$ 2s↑	−14.9785	−15.0278
$S_{2,3}$ 2s↓	−14.9748	−15.0233
$S_{2,3}$ 2p↑	−11.1965	−11.2375
$S_{2,3}$ 2p↓	−11.1919	−11.2320

Table IV. Ground State Total Energies (Ry) and Charge Distribution (electrons) for $S_3^-(1)$ and $S_3^-(2)$

	$S_3^-(1)$	$S_3^-(2)$
Total energy	−2378.010	−2377.489
Kinetic energy	2311.102	2308.929
Potential energy	−4689.109	−4686.414
Total charge in various regions:		
Center sulfur	14.153	13.832
Each terminal sulfur	14.685	14.390
Extramolecular	0.758	0.892
Intersphere	2.492	2.889

Table V. Calculated Electronic Spectra of S_3^-

Transition	Calculated energy, cm^{-1} $S_3^-(1)$	$S_3^-(2)$
$1a_2 \rightarrow 2b_2$	10 501[a]	13 190[a]
$4a_1 \rightarrow 2b_2$	10 512[a]	12 192[b]
$2b_2 \rightarrow 5a_1$	23 264[b]	25 283[b]

[a] These values were calculated to self-consistency using the transition-state procedure.[30c,d] [b] These values were obtained as a first approximation to the electronic transition by taking the difference between the two energy levels involved; however, the transition-state procedure was not employed. The first approximation gives a slightly lower value than that obtained using the transition-state method. For example, for $S_3^-(1)$, a first approximation to the transition $4a_1 \rightarrow 2b_2$ is 10 206 cm^{-1} as compared to 10 512 cm^{-1} by the transition-state procedure.

function at 6561 grid points within the area of the plot. Calculated electronic excitation energies for spin-allowed and symmetry-allowed transitions are given in Table V.

The S_2^- Calculations. Again, the two calculations, $S_2^-(1)$ and $S_2^-(2)$, were performed in spin-unrestricted form because of the open-shell nature of the molecules. Calculated ground state valence orbital energies and charge

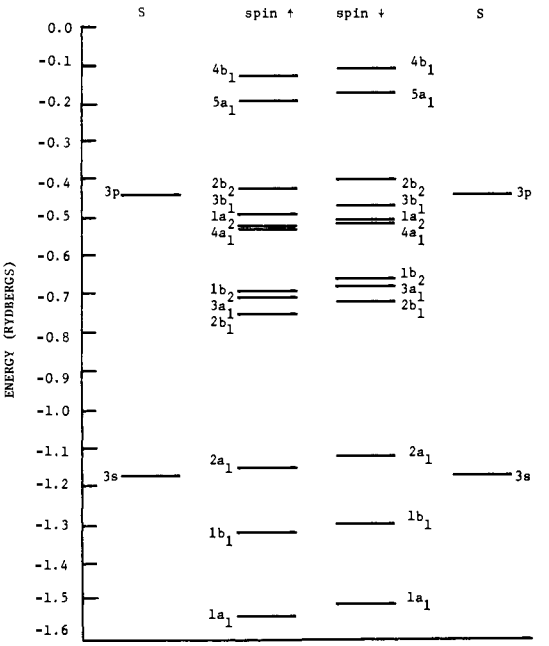

Figure 2. Ground state valence energy levels for the $S_3^-(2)$ ion. Corresponding SCF-Xα energy levels of the free atoms are shown for comparison. The highest occupied level is $2b_2\uparrow$.

distributions are summarized in Table VI. Calculated core one-electron energies are given in Table VII. Spin-polarized SCF-Xα electronic energy levels of the $S_2^-(1)$ ion are shown in Figure 4. The highest occupied level in the ground state is $1\pi_g\downarrow$. Calculated all-electron energies and charge distributions are summarized in Table VIII. A contour map of the one-electron wave function for the highest occupied energy level $1\pi_g\downarrow$ for $S_2^-(1)$ appears as Figure 5. This map has been generated from the numerical values of the wave function at 6561 grid points within the area of the plot. Calculated electronic excitation energies for spin-allowed and symmetry-allowed transitions are given in Table IX.

The S_3^{2-} Calculation. The ground state valence orbital energies and charge distributions for S_3^{2-} are summarized in Table X. Calculated core one-electron energies are given in Table XI. The SCF-Xα electronic energy levels for the ion are shown in Figure 6. The highest occupied level in the ground state is $2b_2$. Summarized in Table XII are the calculated all-electron energies and charge distributions. The energy of the lowest allowed electronic transition, $2b_2 \rightarrow 5a_1$, was calculated self-consistently to be 24 482 cm^{-1}.

Discussion

The Electronic Structure of S_3^-. There is no direct structural information on the S_3^- ion. Walsh's rules[35] or empiri-

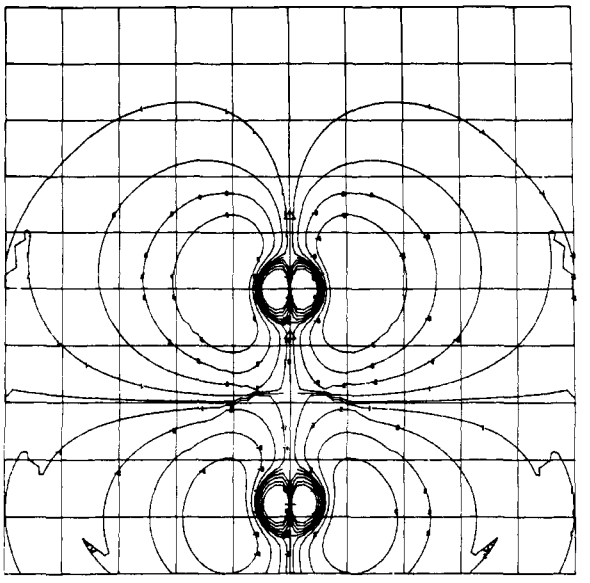

Figure 3. Contour map of the $2b_2\uparrow$ wave function of S_3^-(2). Beginning with the nodal line the contours increase to 0.01, 0.03, 0.06, and 0.10 (electron/bohr^3)$^{1/2}$. The grid is in bohrs; S_1 is at the bottom. Discontinuities are the result of noise in the calculation.

Table VI. Ground State Valence Energy Levels[a] (Ry) and Charge Distribution[b] for S_2^-

Level	Energy S_2^-(1)	Energy S_2^-(2)	% S S_2^-(1)	% S S_2^-(2)
$2\sigma_u\downarrow$	−0.086	−0.153	68.5	71.8
$2\sigma_u\uparrow$	−0.115	−0.182	70.6	72.4
$1\pi_g\downarrow$	−0.353	−0.364	60.7	66.2
$1\pi_g\uparrow$	−0.382	−0.392	61.3	66.8
$1\pi_u\downarrow$	−0.538	−0.508	52.2	57.9
$1\pi_u\uparrow$	−0.553	−0.535	69.3	58.6
$2\sigma_g\downarrow$	−0.566	−0.542	52.8	73.0
$2\sigma_g\uparrow$	−0.583	−0.570	69.7	73.4
$1\sigma_u\downarrow$	−1.066	−1.078	77.6	82.5
$1\sigma_u\uparrow$	−1.098	−1.109	77.8	82.7
$1\sigma_g\downarrow$	−1.304	−1.261	75.9	80.3
$1\sigma_g\uparrow$	−1.336	−1.291	76.1	80.5

[a] The highest occupied level is $1\pi_g\downarrow$. [b] The remainder of the electronic charge is distributed between the intersphere and extramolecular regions (not listed here).

Table VII. Ground State Core Energy Levels (Ry) for S_2^-

Level	Energy S_2^-(1)	Energy S_2^-(2)
$S_{1,2}$ 1s↑	−176.9613	−176.9971
$S_{1,2}$ 1s↓	−176.9561	−176.9721
$S_{1,2}$ 2s↑	−15.0071	−14.9912
$S_{1,2}$ 2s↓	−15.0006	−14.9851
$S_{1,2}$ 2p↑	−11.2157	−11.2022
$S_{1,2}$ 2p↓	−11.2077	−11.1947

cal comparison[38] with the isoelectronic O_3^- and ClO_2 species naturally leads to the expectation that S_3^- must be bent. On the basis of structural data[38] for various S_x^{2-} it was expected that the S–S distance would be ca. 2.10 Å and the angle ca. 110°. In order to test whether the results might depend seriously upon the choice of bond length the calculation was also carried out with a distance of 2.00 Å. Dependence on angle in the range 105–115° was expected to be less than on interatomic distance, so it was decided not to vary the angle unless the dependence on distance proved to be great.

Inspection of Table II and Figure 2 shows that the

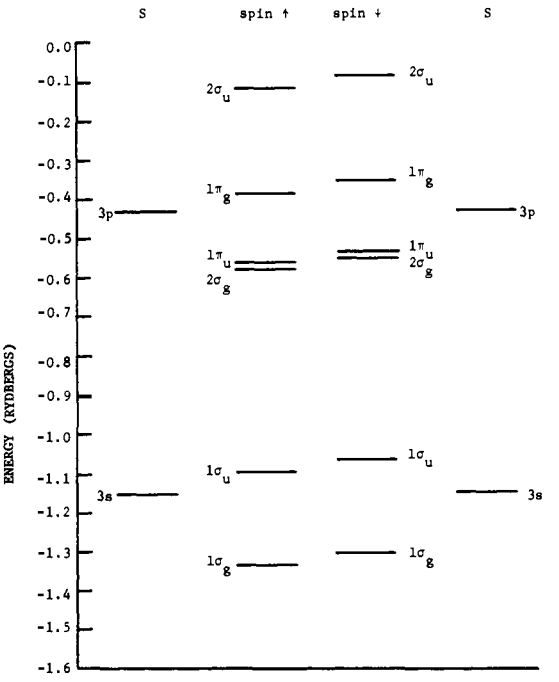

Figure 4. Ground state valence energy levels for S_2^-(1). Corresponding SCF-Xα energy levels of the free atoms are shown for comparison. The highest occupied level is $1\pi_g\downarrow$.

Table VIII. Ground State Total Energies (Ry) and Charge Distribution (electrons) for S_2^-

	S_2^-(1)	S_2^-(2)
Total energy	−1581.358	−1581.654
Kinetic energy	1510.002	1512.214
Potential energy	−3091.360	−3096.869
Total charge in various regions:		
Each sulfur	14.199	14.526
Extramolecular	1.222	0.951
Intersphere	1.817	1.609

Table IX. Calculated Electronic Spectra of S_2^-

Transition	Calculated energy, cm^{-1} S_2^-(1)	Calculated energy, cm^{-1} S_2^-(2)
$1\pi_u \rightarrow 1\pi_g$	20 279[a]	15 846[a]
$1\pi_g \rightarrow 2\pi_u$	29 289[b]	23 111[b]

[a] These values were calculated to self-consistency using the transition-state procedure.[30c,d] [b] These values were obtained as a first approximation to the electronic transition by taking the difference between the two levels involved; however, the transition-state procedure was not employed. Usually the first approximation gives a slightly lower value than that obtained using the transition-state method; however, in this case, the values obtained from the first approximation were exactly those resulting from the transition-state procedure.

ground state valence energy levels for S_3^- fall into four distinct categories. Between −1.60 and −1.10 Ry is a group of levels whose provenance is mainly the 3s atomic orbitals. These levels are not strongly bonding molecular orbitals because the electrons in the 3s shell are tightly bound and do not overlap effectively. The energy levels between −0.75 and −0.60 Ry represent S–S bonding orbitals and are chiefly sulfur 3p-like in origin. The $2b_1$ and $3a_1$ orbitals correspond to $S(3p_z)$–$S(3p_z)$ and $S(3p_x)$–$S(3p_x)$ bonding in the molecular plane. The $1b_2$ levels represent $S(3p_y)$–$S(3p_y)$ bonding perpendicular to the plane of the molecule (as in allylic-type π bonding). The electron density is relatively evenly distributed over the center sulfur and combined ter-

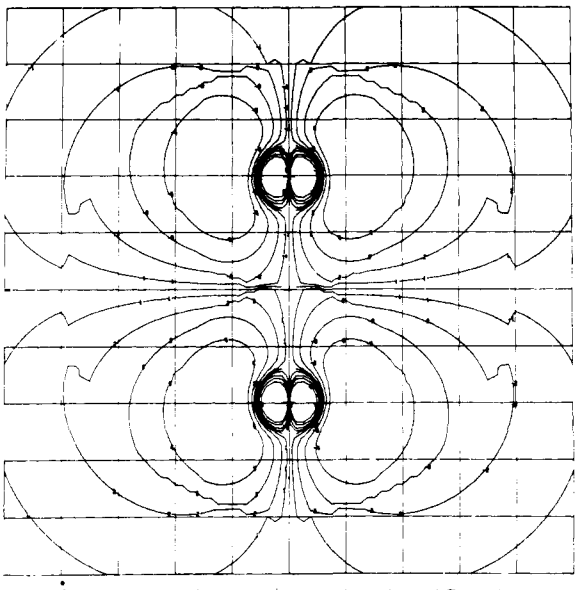

Figure 5. Contour map of the $1\pi_g\downarrow$ wave function of $S_2^-(1)$. Beginning with the nodal line through the origin the contours increase to 0.01, 0.03, 0.06, and 0.10 (electron/bohr^3)$^{1/2}$. The grid is in bohrs. Discontinuities are the result of noise in the calculation.

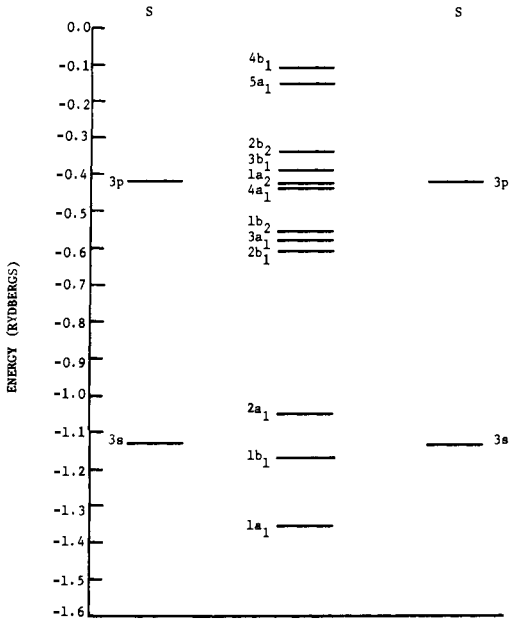

Figure 6. Ground state valence energy levels for S_3^{2-}. Corresponding SCF-Xα energy levels for the free atoms are shown for comparison. The highest occupied level is $2b_2$.

Table **X.** Ground State Energy Levels[a] (Ry) and Charge Distribution[b] for S_3^{2-}

Level	Energy	% S_1	% $S_{2,3}$
$4b_1$	−0.114	26.4	31.6
$5a_1$	−0.150	14.9	25.8
$2b_2$	−0.343	28.1	36.3
$3b_1$	−0.389	1.1	67.1
$1a_2$	−0.427	0.6	62.9
$4a_1$	−0.441	7.1	55.1
$1b_2$	−0.559	31.1	24.9
$3a_1$	−0.584	34.8	31.9
$2b_1$	−0.614	31.4	42.0
$2a_1$	−1.049	29.0	52.7
$1b_1$	−1.174	4.6	78.3
$1a_1$	−1.356	47.6	32.7

[a] The highest occupied level is $2b_2$. [b] The remainder of the electronic charge is distributed between the intersphere and extramolecular regions (not listed here).

Table **XI.** Ground State Core Energy Levels (Ry) for S_3^{2-}

Level	Energy	Level	Energy
S_1 1s	−177.1728	$S_{2,3}$ 1s	−176.9586
S_1 2s	−15.0627	$S_{2,3}$ 2s	−14.9266
S_1 2p	−11.2796	$S_{2,3}$ 2p	−11.1367

Table **XII.** Ground State Total Energies (Ry) and Charge Distribution (electrons) for S_3^{2-}

Total energy	−2371.729
Kinetic energy	2271.897
Potential energy	−4643.625
Total charge in various regions:	
Center sulfur	14.307
Each terminal sulfur	14.841
Extramolecular	1.012
Intersphere	4.999

minal sulfur regions. In the range −0.55 to −0.45 Ry are three essentially nonbonding molecular orbitals. The $4a_1$ and $3b_1$ levels may be described as nonbonding orbitals in the plane of the molecule, while the $1a_2$ level is a nonbonding orbital in the perpendicular plane. In all of these three orbitals, the electronic density is mainly concentrated on the terminal atoms. A very small d_{xy} contribution from the center sulfur is also observed. The $2b_2$, $5a_1$, and $4b_1$ levels in the range −0.45 and −0.10 Ry are the antibonding counterparts of S-S bonding orbitals of the same symmetry ($1b_2$, $3a_1$, and $2b_1$) and, like them, give a fairly even distribution of electronic density over the center sulfur and combined terminal sulfur regions. The $2b_2\uparrow$ and $2b_2\downarrow$ orbitals are the highest occupied and lowest unoccupied levels in the ion. The antibonding character of the $2b_2$ level is readily seen from the contour map in Figure 3. The region of zero electron density between the π orbitals of the two sulfur atoms precludes any orbital overlap or bonding interaction.

The energy-level diagram for $S_3^-(1)$ differs only slightly from that for $S_3^-(2)$. The expected qualitative effect of shifting all the energy levels downward in $S_3^-(2)$ due to the differences in sphere radii and bond lengths is observed, but the quantitative change is quite small, and the level spacings remain practically identical. The free-atom energy levels for sulfur are the same in both cases. The effect of the decreased bond length and smaller sphere radii lowers the total energy by 0.521 Ry, or 0.02%. The total charge distribution is altered by a slight decrease in the number of electrons within the atomic regions and a slight increase in the number of electrons within the intersphere and extramolecular regions in going from $S_3^-(1)$ to $S_3^-(2)$. However, it is clear that the main, semiquantitative, chemically significant results are not sensitive to the variation in S-S bond length from 2.00 to 2.10 Å. It is thus also not to be expected that a change in the bond angle by ±5° (i.e., to 105 or 115°) would have any important effect on the results.

The Electronic Structure of S_2^-. Again, the sensitivity of the results to choice of bond distance was tested since the exact S-S distance is not known.

Inspection of Table VI and Figure 4 shows that the ground state valence energy levels for S_2^- can be considered in three categories. Between −1.50 and −1.35 Ry are the energy levels $1\sigma_g$ and $1\sigma_u$ whose provenance is principally the sulfur 3s levels. In the range −0.60 to −0.50 Ry are the $2\sigma_g$ orbital, which is mainly a $S(3p_z)$-$S(3p_z)$ bonding orbital, and the $1\pi_u$ orbital which may be described as mainly a $S(3p_{x,y})$-$S(3p_{x,y})$ bonding orbital, and the $1\pi_u$ orbital

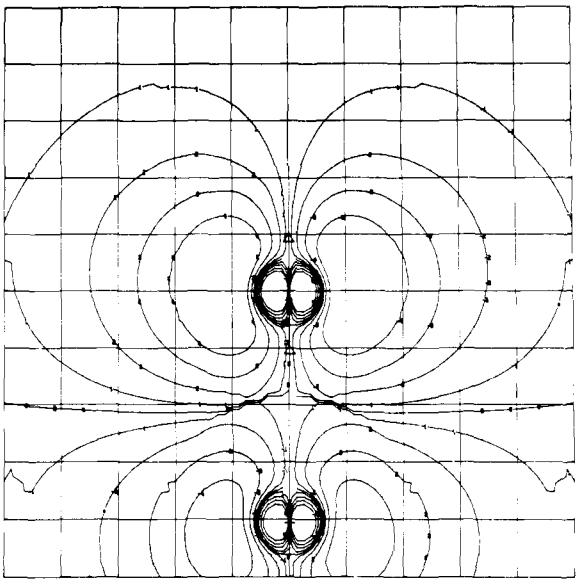

Figure 7. Contour map of the $2b_2$ wave function of S_3^{2-}. Beginning with the nodal line between the atoms the contours increase to 0.01, 0.03, 0.06, and 0.10 (electron/bohr^3)$^{1/2}$. The grid is in bohrs. Discontinuities are the result of noise in the calculations.

which may be described as mainly a $S(3p_{x,y})$-$S(3p_{x,y})$ bonding level. The antibonding counterparts, namely $1\pi_g$ and $2\sigma_u$, are in the range −0.50 to −0.40 Ry. The $1\pi_g\downarrow$ and $2\pi_u\uparrow$ orbitals are the highest occupied and lowest unoccupied levels in the ion. The antibonding character of the $1\pi_g\downarrow$ orbital, which has a node between the nuclei, is clearly seen from the contour map, Figure 5.

Comparison of energy-level diagrams for $S_2^-(1)$ and $S_2^-(2)$ shows no significant differences. The expected qualitative effects of shifting all the energy levels upward in $S_2^-(2)$ due to the differences in sphere radii and bond lengths is observed, but the quantitative change is quite small, and the level spacings remain constant. The free-atom energy levels for sulfur are the same in both cases. The effect of the increased bond length and larger sphere radii raises the total energy by 0.296 Ry, or 0.02%. The total charge distribution is altered by a slight increase in the number of electrons within the atomic regions and a slight decrease in the number of electrons in the intersphere and extramolecular regions in going from $S_2^-(1)$ to $S_2^-(2)$.

The Electronic Structure of S_3^{2-}. Inspection of Table X and Figure 6 shows that the ground state valence energy levels for S_3^{2-} are, as expected, very similar to those for the S_3^-, ion, and the comments previously made are applicable here as well. The expected qualitative effects of shifting all the energy levels upward in S_3^{2-} because of the extra electron is observed, but the quantitative change is small. The orbital spacing and ordering remain constant. The free-atom energy levels for sulfur also increase by a small amount in going from S_3^- to S_3^{2-}. The effect of the added charge on S_3^{2-} lowers the total energy by approximately 6.021 Ry, or 0.25%. The total charge distribution is altered by a slight increase in the number of electrons within the atomic regions because of the increased charge. This results in a decrease in the number of electrons within the intersphere and extramolecular regions. The contour maps of the $2b_2$ levels of S_3^- and S_3^{2-} are very similar.

Electronic Spectra. The optical absorption spectrum of the S_3^{2-} ion in aqueous solution has been investigated by Giggenbach,[23] who finds two bands, at about 24 000 and 33 000 cm^{-1}. Because the positions and shapes of these bands were obtained by deconvoluting complex superposed spectra of several S_x^{2-} species using equilibrium constants which are imprecise, both the peak positions and band widths are less accurately known than one ordinarily expects. The lowest symmetry-allowed electronic transition for S_3^{2-} should be due to the orbital excitation $b_1 \rightarrow a_1$, meaning that the transition is $B_1 \leftarrow A_1$. A significant increase in the S-S-S angle for the $^1B_1$ state compared to the $^1A_1$ ground state might be anticipated from the Walsh diagram[35] so that Franck-Condon forbiddenness would tend to lower the intensity. Giggenbach's assignments of the 24 000-cm^{-1} peak to the $^1B_1 \leftarrow {}^1A_1$ transition and the 33 000-cm^{-1} peak to the $^1B_2 \rightarrow {}^1A_1$ transition appear very reasonable.

Table XIII. Comparison of Calculated Electronic Transition Energies to Experimental Values of Peak Positions and O–O Bands

Molecule	Transition	Calcd value (cm^{-1})	Estimated O–O position (cm^{-1})	Exptl peak position (cm^{-1})
$S_3^-(1)$	$1a_2 \rightarrow 2b_2$	10 501		
			13 500	16 000
$S_3^-(2)$	$1a_2 \rightarrow 2b_2$	13 190		
$S_2^-(1)$	$1\pi_u \rightarrow 1\pi_g$	20 279		
			21 000	24 000
$S_2^-(2)$	$1\pi_u \rightarrow 1\pi_g$	15 846		

We predict the energy of the $^1B_1 \leftarrow {}^1A_1$ ($2b_2 \rightarrow 5a_1$) transition to be 24 500 cm^{-1}. In view of the uncertainties in estimating the experimental band peak, mentioned above, and the fact that Franck-Condon effects render the position of the O–O component uncertain, we feel that the agreement with experiment is satisfactory and that this result indicates that our method of calculation is reliable for polysulfide anions.

We therefore turn to a comparison of calculated electronic transition energies with observed spectra for the radical anions S_2^- and S_3^-. These comparisons are made in Table XIII. It must be noted first that we are dealing, experimentally, with band envelopes formed by unresolved vibrational progressions and that the band peaks do not correspond to the energy of purely electronic excitation. Instead, the energy of the transition without accompanying vibrational excitation, which is what we are attempting to calculate, should lie approximately at the low-frequency edge of the band envelope. Thus, in Table XIII we give the band maxima and also the estimated energies for the vibrational O–O transition. These are obtained from the spectrum shown in Figure 8.

Second, we note that for S_3^- the lowest energy transition, $3b_1 \rightarrow 2b_2$ is not orbitally allowed. The first orbitally allowed transition is $1a_2 \rightarrow 2b_2$ ($^2A_2 \leftarrow {}^2B_2$) with x polarization. For S_2^- the lowest energy transition, $1\pi_u \rightarrow 1\pi_g$ ($^2\pi_u \leftarrow {}^2\pi_g$), is allowed. It is these two allowed transitions that we wish to compare with the reported visible spectra.

Our results clearly show that over the range of S-S distances (2.00-2.25 Å) within which the correct values must lie, the lowest energy transitions for S_3^- and S_2^- are always in the energy order $\nu(S_2^-) > \nu(S_3^-)$, and the separation is consistently about 9500 cm^{-1}. Thus, we conclude that since the S_2^- and S_3^- ions together (Figure 8) give rise to bands separated by 8000 cm^{-1}, we must assign the higher energy band to S_2^- and the lower energy one to S_3^-. This, in turn indicates that the ubiquitous blue chromophore discussed in the introduction is S_3^- and not S_2^-.

The extent to which quantitative agreement can be obtained between the calculated and observed transitions depends on the sulfur-sulfur bond distances used in the calculations. From the vibrational frequencies of S_2^- and S_3^- in alkali halide crystals, given by Holzer et al.,[26] we estimate,

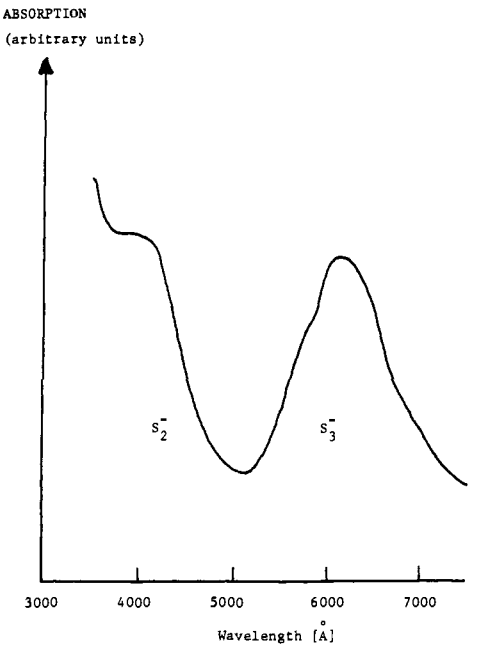

Figure 8. Visible absorption spectrum of an alkali halide crystal containing both S_2^- and S_3^- ions, adapted from Holzer et al.[26]

using a simple valence force field for the latter, that the S-S stretching force constants are very similar in the two cases, namely, about 3.30 ± 0.05 mdyn/Å. Thus the S-S distances in the two ions should be similar. Since a recent study[39] suggests that the S-S distance in S_2^{2-} is greater than that in S_3^{2-}, the same is likely to be true for S_2^- relative to S_3^-. If we assume that for S_3^- the distance is in the range 2.05-2.10 Å, the energy of the first allowed transition is predicted to be 12 000-13 200 cm^{-1} as compared to an observed value of ca. 13 500 cm^{-1}. If for S_2^- we assume that the S-S distance is in the range 2.10-2.20 Å, the energy of the first allowed transition is predicted to be in the range 17 300-20 300 cm^{-1} as compared to the experimental value of ca. 21 000 cm^{-1}. This good agreement of the individual energies, as well as their difference, adds credence to the validity of the calculations and hence to the identification of the S_3^- ion as the source of the blue color of lapis lazuli, ultramarines, and a multitude of other sulfur-containing systems.

Acknowledgments. We are grateful to Professor J. G. Norman, Jr., of the University of Washington for his very generous guidance in the use of the computer programs. We thank the Robert A. Welch Foundation for financial support under Grants A106 and A494.

References and Notes

(1) See, for example, A. F. Wells, "Structural Inorganic Chemistry", 3d ed, Oxford University Press, London, 1962, p 816.
(2) C. Nollner, *Pogg. Ann.*, **98**, 189 (1856).
(3) C. F. Geitner, *Pharm. Ann.*, **129**, 350 (1864).
(4) W. Giggenbach, *Inorg. Chem.*, **10**, 1306 (1971).
(5) G. Delarue, *Bull. Soc. Chim. Fr.*, 1654 (1960).
(6) D. M. Gruen, R. L. McBeth, and A. J. Zielen, *J. Am. Chem. Soc.*, **93**, 6691 (1971).
(7) H. Lux, S. Benninger, and E. Bohm, *Chem. Ber.*, **101**, 2485 (1968).
(8) W. Giggenbach, *J. Inorg. Nucl. Chem.*, **30**, 3189 (1969).
(9) H. Lux and A. Anslinger, *Chem. Ber.*, **94**, 1161 (1961).
(10) W. Giggenbach, *Inorg. Chem.*, **10**, 1308 (1971).
(11) M. V. Merritt and D. T. Sawyer, *Inorg. Chem.*, **9**, 211 (1970).
(12) R. Bonnaterre and G. Cauquis, *J. Chem. Soc., Chem. Commun.*, 293 (1972).
(13) L. Schneider, B. Dischler, and A. Rauber, *Phys. Status Solidi*, **13**, 141 (1966).
(14) J. Suwalski and H. Seidel, *Phys. Status Solidi*, **13**, 159 (1966).
(15) R. P. Martin, W. H. Doub, J. L. Roberts, Jr., and D. T. Sawyer, *Inorg. Chem.*, **12**, 1921 (1973).
(16) T. Chivers and J. Drummond, *Inorg. Chem.*, **11**, 2525 (1972).
(17) T. Chivers, *Nature (London)*, **252**, 32 (1974).
(18) U. Hofmann, E. Herzenstiel, E. Schonemann, and K. Schwarz, *Z. Anorg. Allg. Chem.*, **367**, 119 (1969).
(19) A. Teder, *Ark. Kemi*, **31**, 173 (1969).
(20) G. Schwarzenbach and A. Fischer, *Helv. Chim. Acta*, **43**, 1365 (1960).
(21) J. Greenberg, B. R. Sundheim, and D. M. Gruen, *J. Chem. Phys.*, **29**, 461 (1958).
(22) F. G. Bodewig and J. A. Plambeck, *J. Electrochem. Soc.*, **117**, 904 (1970).
(23) W. Giggenbach, *J. Chem. Soc., Dalton Trans.*, 729 (1973).
(24) T. Matsunaga, *Can. J. Chem.*, **38**, 310 (1960).
(25) K. H. Schwarz and U. Hofmann, *Z. Anorg. Allg. Chem.*, **378**, 152 (1970).
(26) W. Holzer, W. F. Murphy, and H. J. Bernstein, *J. Mol. Spectrosc.*, **32**, 13 (1969).
(27) J. Rolfe, *J. Chem. Phys.*, **49**, 4193 (1968).
(28) L. E. Vanotti and J. R. Morton, *Phys. Rev.*, **161**, 282 (1967).
(29) J. R. Morton, 15th Colloque A.M.P.E.R.E. Grenoble, Sept 1968.
(30) (a) J. C. Slater and K. H. Johnson, *Phys. Rev. B*, **5**, 844 (1972); (b) K. H. Johnson, J. G. Norman, Jr., and J. W. D. Connolly, "Computational Methods for Large Molecules and Localized States in Solids", Plenum Press, New York, N.Y., 1972; (c) K. H. Johnson, *Adv. Quantum Chem.*, **7**, 143 (1973); (d) J. C. Slater, *ibid.*, **6**, 1 (1972); (e) K. H. Johnson and F. C. Smith, Jr., *Phys. Rev. B*, 5, 831 (1972).
(31) K. Schwarz, *Phys. Rev. B*, 5, 2466 (1972).
(32) J. G. Norman, Jr., *J. Chem. Phys.*, **61**, 4630 (1974).
(33) R. E. Watson, *Phys. Rev.*, **111**, 1108 (1958).
(34) J. C. Slater, T. M. Wilson, and J. H. Wood, *Phys. Rev.*, **179**, 28 (1969).
(35) A. D. Walsh, *J. Chem. Soc.*, 2266 (1953).
(36) S. C. Abrahams, *Acta Crystallogr.*, **7**, 432 (1954).
(37) W. S. Miller and A. J. King, *Z. Kristallogr., Kristallgeom., Kristallphys., Kristallchem.*, **94**, 441 (1936).
(38) F. A. Cotton and G. Wilkinson, "Advanced Inorganic Chemistry", 3d ed., Interscience, New York, N.Y., 1972.
(39) S. Yamaoka, J. T. Lemley, J. M. Jenks, and H. Steinfink, *Inorg. Chem.*, **14**, 129 (1975).